Multi-stage Alzheimer's disease diagnosis using Diffusion Tensor Imaging and Cost-Sensitive Machine Learning

Ali KHAZAEE, Abdolreza MOHAMMADI

Department of Electrical Engineering, University of Bojnord, Bojnord, Iran

khazaee.a@gmail.com, a.mohammadi@ub.ac.ir

Abstract: Early and accurate diagnosis of Alzheimer's disease (AD) stages, including Early and Late Mild Cognitive Impairment (EMCI, LMCI), is crucial for intervention. This study leverages Diffusion Tensor Imaging (DTI) metrics from 57 brain regions to classify AD progression and differentiate from healthy controls (HC). The proposed method, which incorporates various machine learning models, Bayesian hyperparameter optimization, 10-fold cross-validation, and cost-sensitive learning, achieved a high test accuracy of 90.4%. Feature ranking consistently identified Axial Diffusivity in the left uncinate fasciculus as a key biomarker, alongside important contributions from the sagittal stratum and hippocampal cingulum. Our findings demonstrate the significant potential of the DTI-derived features combined with optimized machine learning for enhancing multi-stage AD diagnosis and understanding the underlying neuropathological mechanisms.

Keywords: Diffusion Tensor Imaging (DTI), Alzheimer’s Disease (AD), Early Mild Cognitive Impairment (EMCI), Late Mild Cognitive Impairment (LMCI), Bayesian Optimization, Cost-Sensitive Machine Learning.

1. Introduction

Diffusion Tensor Imaging (DTI), Diffusion-Weighted Imaging (DWI), and Magnetic Resonance Imaging (MRI) are interconnected imaging modalities that collectively contribute to understanding brain structure and function. MRI serves as the foundational imaging technique, producing high-resolution anatomical images of the brain using strong magnetic fields and radio waves. Building upon MRI, DWI measures the diffusion of water molecules within tissues, capturing the random Brownian motion of water (Basser, Mattiello, & LeBihan, 1994). DTI extends DWI by modeling the directional movement of water molecules, enabling the assessment of anisotropic diffusion in the white matter tracts. Through the tensor model, DTI provides additional metrics, such as fractional anisotropy (FA) and mean diffusivity (MD), which reflect the orientation and integrity of the white matter fibers. Thus, while DWI and MRI provide general and diffusion-sensitive imaging, DTI focuses on the directional and structural properties of the white matter, making it a crucial tool for studying brain connectivity and microstructural changes in various neurological conditions (Le Bihan et al., 2001).

Alzheimer's Disease (AD) is a progressive neurodegenerative disorder characterized by cognitive decline, memory loss, and behavioral changes, ultimately impairing daily functioning (Jack et al., 2010). It is widely recognized as the most common cause of dementia, and its progression occurs across distinct clinical stages. Early Mild Cognitive Impairment (EMCI) and Late Mild Cognitive Impairment (LMCI) represent transitional phases between healthy aging and the onset of Alzheimer’s dementia (Petersen et al., 1999). EMCI is an initial stage characterized by subtle memory impairments and minimal interference with daily life, often serving as a precursor to a more pronounced cognitive decline. LMCI is a more advanced stage of impairment, where individuals experience noticeable deficits in memory, language, or executive function, though their ability to perform daily activities remains relatively preserved (Albert et al., 2011). Differentiating these stages from health controls (HC) is crucial for the early diagnosis and intervention, as all therapeutic strategies are most effective during the preclinical and prodromal phases. Advanced imaging modalities, such as MRI and DTI, along with the machine learning techniques, offer promising avenues for identifying the subtle brain changes associated with these stages. The distinctions are essential for tracking the disease progression, the understanding underlying the pathophysiology, and tailoring interventions to the specific stages of AD (Sperling et al., 2011).

https://doi.org/10.33436/v35i2y202506

DTI provides valuable quantitative metrics that reflect the microstructural integrity of the white matter, which are instrumental in studying the neurodegenerative diseases such as AD (Chandra, Dervenoulas, & Politis, 2019). Among these metrics, FA measures the degree of the directional water diffusion, serving as an indicator of the white matter coherence and fiber integrity. MD quantifies the overall magnitude of water diffusion, offering insights into the density and structural organization of the brain tissue. Axial Diffusivity (AxD) reflects water diffusion along the principal axis of the white matter tracts, often associated with the axonal integrity, while Radial Diffusivity (RD) measures the diffusion perpendicular to the primary axis, linked to the myelin integrity. By capturing the stage-specific microstructural abnormalities, these metrics enable the differentiation of the healthy controls from the individuals at various stages of disease progression. Combining these biomarkers by advanced computational techniques, such as machine learning, can enhance the diagnostic accuracy and provide a deeper understanding of the underlying pathophysiological changes in AD. This study aims to leverage FA, MD, AxD, and RD derived from DTI data to identify and classify the stages of EMCI, LMCI, and AD, providing a non-invasive and sensitive approach for an early detection and monitoring of the disease.

To achieve an accurate classification of the AD stages, including EMCI and LMCI, the advanced machine learning methods are essential for analyzing the complex neuroimaging data (Khazaee, Ebrahimzadeh, & Babajani-Feremi, 2015; Khazaee, Ebrahimzadeh, & Babajani-Feremi, 2017; Hojjati et al., 2018). This study employs a diverse set of classification algorithms, including decision trees, discriminant analysis, logistic regression classification, Naïve bayes classifiers, support vector machines (SVM), efficiently trained linear classifiers, nearest neighbor classifiers, kernel approximation classifiers, and ensemble classifiers. Each algorithm offers unique advantages, such as interpretability (e.g., decision trees and logistic regression), adaptability to high-dimensional data (e.g., SVM and ensemble classifiers), and computational efficiency (e.g., Naïve bayes and linear classifiers). By leveraging this comprehensive approach, the study aims to evaluate the performance of each classifier in distinguishing between HC and different stages of AD using the DTI-derived metrics such as FA, MD, AxD, and RD. The integration of the multiple classifiers ensures robustness and provides insights into the most effective techniques for identifying subtle patterns in neuroimaging data. The ensemble methods, in particular, combine the strengths of the individual classifiers, enhancing predictive accuracy and reliability. This methodological diversity underscores the study's potential to contribute novel, evidence-based solutions for early and precise identification of the AD stages, ultimately supporting timely clinical interventions.

In addition, the Bayesian optimization was used to find the optimum values of the different classification models, enhancing their predictive performance and ensuring the most accurate classification of the AD stages. This optimization process involved fine-tuning hyperparameters to strike a balance between the model complexity and generalizability. Cost-sensitive learning was used to overcome imbalanced data and to prevent misclassification of the minority classes. Different feature ranking methods such as Minimum Redundancy Maximum Relevance (MRMR), Chi-Square (Chi2), Analysis of Variance (ANOVA), and Kruskal-Wallis were employed to identify the most informative features and the regions of the brain most affected at different stages of the AD. These methods provided complementary insights, with MRMR focusing on mutual information, Chi2 emphasizing statistical independence, ANOVA examining variance among groups, and Kruskal-Wallis assessing the non-parametric differences. By integrating these diverse techniques, the study aimed to pinpoint the key biomarkers and neural pathways involved in the progression from HC to EMCI, LMCI, and AD. This multifaceted approach not only improved classification accuracy but also advanced the understanding of the underlying neuropathological mechanisms, thereby contributing to the development of the targeted interventions and personalized treatment strategies.

The remainder of this paper is organized as follows: Section 2 describes the dataset, imaging protocols, DTI metrics, classification techniques, and the cost-sensitive learning strategy applied to address class imbalance. Section 3 presents the experimental results, including model performance, feature ranking, and test evaluation. Section 4 provides a detailed discussion of the findings. Finally, Section 5 concludes the paper and outlines future research directions.

2. Methods

2.1. Subjects

The "USC - DTI ROI Summary Measures v1" dataset, derived from the ADNI (ADNIGO, ADNI2), provides preprocessed DTI metrics for analyzing the microstructural properties of the white matter tracts in the brain. This dataset is ideal for studying the neurodegenerative diseases, particularly Alzheimer's disease, and related conditions. The subjects include those with normal cognition, EMCI, LMCI, and AD, facilitating the exploration of the white matter changes across the spectrum of the cognitive decline. The rigorous preprocessing and atlas-based regions of interest (ROIs) methodology ensure high-quality and consistent metrics suitable for group-level analyses (Nir et al., 2013). This dataset includes 976 records, however, the number of image data for two classes, namely mild cognitive impairment (MCI) and Significant Memory Concern (SMC), was too small to include them in the experiments. So, the resulting dataset contains 886 images divided into four classes: 164 images of AD patients, 165 of LMCI, 337 of EMCI, and 220 of HC.

This dataset uses 57 ROIs defined by the Johns Hopkins University (JHU) DTI atlas (Mori et al., 2008). In addition to the 52 JHU labels, 5 more ROIs were evaluated: the bilateral fornix, bilateral genu, bilateral body and bilateral splenium of the corpus callosum, as well as the full corpus callosum, to get full summary measures of these regions. These ROIs encompass critical white matter tracts, including the corpus callosum (genu, body, splenium), corona radiata (anterior, superior, posterior), cingulum, uncinate fasciculus, thalamic radiations, and other major tracts. These tracts are widely recognized for their involvement in the cognitive processing and have been repeatedly associated with the AD pathology. For example, the microstructural degeneration in the uncinate fasciculus and cingulum bundle has been linked to the early episodic memory decline, while the damage to the corpus callosum and thalamic radiations has been observed in both MCI and AD stages. The selection of these ROIs thus allows a focused analysis of the white matter pathways most susceptible to the AD-related neurodegeneration. To ensure quality, artifacts in four ROIs were excluded when they fell outside the imaging field of view (Nir et al., 2013).

2.2. Image acquisition and preprocessing

The imaging data were acquired using 3.0 Tesla MRI scanners following standardized ADNI protocols. High-resolution DWI were collected using a dual-spin echo echo-planar imaging sequence with a b-value of 1,000 s/mm² across 41 non-collinear diffusion directions and 5 b0 images. Slice thickness was set to 2.7 mm with an in-plane voxel size of 2.7 × 2.7 mm², resulting in a total scan time of approximately 9 minutes (Jack et al., 2008; Nir et al., 2013).

Preprocessing involved rigorous quality assurance steps to ensure robust data analysis. Corrections for head motion and eddy current distortions were performed using FSL's eddy-correct tool (Jenkinson, Bannister, Brady, & Smith, 2002). The non-brain tissue was removed from the diffusion-weighted images and T1-weighted anatomical scans using the Brain Extraction Tool (BET) (Smith, 2002) and ROBEX (Iglesias et al., 2011). A spatial normalization of T1-weighted images to the Colin27 brain template was performed using FSL's FLIRT with 6 degrees of freedom (Holmes et al., 1998). To correct for susceptibility-induced distortions at tissue-fluid interfaces, b0 images were elastically aligned to their T1-weighted counterparts using mutual information-based registration (Leow et al., 2007).

2.3. Diffusion tensor imaging measures and their importance

The four key DTI measures—FA, MD, AxD, and RD—are calculated from the eigenvalues ($\lambda 1$, $\lambda 2$, $\lambda 3$) of the diffusion tensor, which describe water diffusion along the three principal axes of the diffusion ellipsoid.

FA is a scalar value representing the degree of diffusion anisotropy and is calculated as:

$$FA = \sqrt{\frac{3}{2}} \cdot \frac{\sqrt{(\lambda_1 - \bar{\lambda})^2 + (\lambda_2 - \bar{\lambda})^2 + (\lambda_3 - \bar{\lambda})^2}}{\sqrt{\lambda_1^2 + \lambda_2^2 + \lambda_3^2}} \quad (1)$$

Where $\bar{\lambda} = (\lambda_1 + \lambda_2 + \lambda_3)/3$ is the mean diffusivity. FA ranges from 0 (isotropic diffusion) to 1 (highly anisotropic diffusion), reflecting the coherence of the white matter fibers. FA is sensitive to the structural changes in the brain and is widely used in studying AD, where the lower FA values often correlate with a cognitive decline and disease progression (Stebbins & Murphy, 2009).

MD is the average of the eigenvalues, providing a measure of overall water diffusion within a voxel:

$$MD = \frac{\lambda_1 + \lambda_2 + \lambda_3}{3} \quad (2)$$

This measure reflects the tissue density and integrity, with higher MD values indicating microstructural degradation. Increased MD values indicate neuronal loss, tissue degeneration, or extracellular matrix expansion, common in neurodegenerative diseases (Le Bihan et al., 2001). In Alzheimer's disease, elevated MD values in the white matter regions suggest a progressive tissue breakdown and reduced microstructural complexity (Acosta-Cabronero et al., 2012).

AxD represents diffusion along the principal axis of the diffusion ellipsoid, aligned with the primary direction of the white matter tracts, and is calculated as:

$$AxD = \lambda_1 \quad (3)$$

Changes in the AxD values are often associated with an axonal damage or disruption of the core structure of the white matter fibers (Song et al., 2002). A decreased AxD is commonly observed in the conditions involving axonal injury, such as traumatic brain injury or advanced stages of the AD. While the AxD provides specific insights into the axonal health, its interpretation often requires a comparison with RD and FA to comprehensively understand the underlying pathology.

RD is the average of the diffusion perpendicular to the principal axis and is calculated as:

$$RD = \frac{\lambda_2 + \lambda_3}{2} \quad (4)$$

The increased RD values are typically associated with the demyelination or compromised insulation of axons, as seen in the neurodegenerative diseases and conditions involving white matter disruption (Sun et al., 2006). In the Alzheimer's disease, higher RD values in specific tracts have been linked to myelin loss and white matter degradation, contributing to cognitive impairments (Stebbins & Murphy, 2009).

These four key scalar measures derived from DTI offer complementary information about the white matter structure and its alterations due to neurological and neurodegenerative conditions. Each of these measures provides a distinct perspective on the underlying biophysical properties of the white matter, making them essential tools for studying brain connectivity and pathology (Le Bihan et al., 2001; Mori & Zhang, 2006).

2.4. Classification methods

To classify the AD stages and differentiate them from the healthy controls, a comprehensive set of machine learning classifiers was employed. These classifiers were implemented using MATLAB's Classification Learner App and custom scripts for optimized performance and interpretability. The classifiers were selected to explore a diverse range of algorithms, covering tree-based models, discriminant analysis, logistic regression, Naïve Bayes classifiers, SVMs, nearest neighbor algorithms, kernel approximation methods, and ensemble learning techniques. Each approach offers unique advantages for handling the complexity of the high-dimensional DTI data.

Decision Trees, including Fine Tree, Medium Tree, and Coarse Tree models, provide a hierarchical structure for classification by recursively splitting the data based on feature thresholds. These models differ in the maximum number of splits, where Fine Trees allow numerous splits to capture fine-grained patterns, while Coarse Trees limit splits for simplicity and generalization. *Linear Discriminant Analysis (LDA)* was used to find linear boundaries that separate different diagnostic categories based on the DTI features. LDA is computationally efficient and effective for linearly separable datasets. *Logistic Regression Classification*, particularly Efficient Logistic Regression, estimates class probabilities using a logistic function, making it ideal for probabilistic classification tasks and robust to outliers when combined with regularization techniques (Hosmer Jr, Lemeshow & Sturdivant, 2013). *Gaussian Naïve Bayes and Kernel Naïve Bayes* classifiers assume feature independence and apply Bayes' theorem for classification. These classifiers are computationally efficient and well-suited for datasets with limited inter-feature dependencies (Rish, Hellerstein & Thathachar, 2001). A variety of *SVM models* were explored, including Linear, Quadratic, Cubic, Fine Gaussian, Medium Gaussian, and Coarse Gaussian SVMs . Gaussian SVMs use radial basis functions (RBFs) to capture non-linear relationships in the data, with varying kernel widths (e.g., Fine, Medium, and Coarse) to control flexibility. SVMs are particularly effective for high-dimensional datasets with a clear margin of separation. The *Nearest Neighbor (KNN) classifiers*, including Fine KNN, Medium KNN, Coarse KNN, Cosine KNN, Cubic KNN, and Weighted KNN, predict class labels based on the proximity of the data points in the feature space. *Kernel Approximation Classifiers*, including SVM Kernel and Logistic Regression Kernel models, map the input data into higher-dimensional spaces using kernel functions to capture non-linear relationships. These approximations allow for efficient training and prediction while preserving the benefits of kernelized models (Rahimi & Recht, 2007). The *ensemble learning methods*, such as Boosted Trees, Bagged Trees, Subspace Discriminant, Subspace KNN, and RUSBoosted Trees, combine multiple base learners to improve classification accuracy. The subspace methods enhance diversity by training learners on random subsets of features, and the RUSBoosted Trees tackle imbalanced datasets by undersampling the majority class during training (Seiffert et al., 2010).

2.5. Cost-Sensitive Learning for Addressing Class Imbalance

To mitigate the challenges posed by an imbalanced dataset, where certain classes are significantly underrepresented, a cost-sensitive learning approach was adopted through the design of a custom cost matrix. The rationale behind this method is to explicitly penalize misclassifications of the minority classes more heavily than those of the majority classes, thereby guiding the learning algorithm to focus its optimization efforts on the less frequent, yet often critical, categories. Specifically, the entries in the cost matrix were derived from the inverse of each class's frequency within the training data, followed by normalization. This ensures that classes with fewer samples are assigned a proportionally higher misclassification cost, while correct classifications (represented by the diagonal elements of the matrix) incur no cost. By integrating these differential costs into the model's training process, the objective is to reduce the bias towards the majority classes and achieve a more balanced predictive performance across all categories, particularly enhancing the classification accuracy for the minority classes.

3. Results

The dataset consisted of 886 images categorized into four diagnostic groups: 164 images from AD patients, 165 from LMCI subjects, 337 from EMCI subjects, and 220 from HC. To ensure a strict separation between the training and testing phases, we reserved 20% of the data as a completely independent hold-out test set, which was not used in any way during the model training or validation. The remaining 80% of the data was used exclusively for the model development, where we applied 10-fold cross-validation to train and validate the classifiers. In this procedure, the training data were partitioned into ten subsets; in each fold, nine subsets were used for training and one subset for validation, cycling through all subsets to obtain robust estimates of the model performance and to minimize overfitting. This approach guarantees that the test set remains entirely

unseen during the entire training and hyperparameter tuning process. After the model was finalized based on cross-validation, it was evaluated on the independent 20% hold-out test set, providing an unbiased and rigorous estimate of its accuracy on unseen data. While an external validation on a separate dataset would further strengthen the findings, the use of a strictly held-out test set offers a reliable assessment of the model generalizability, mitigating concerns of overfitting and data leakage.

The input features consisted of averaged values of FA, AxD, MD, and RD over 57 ROIs, resulting in 228 features used for training the machine learning models. Figure 1 illustrates the overall procedure of the proposed method. Table 1 presents the obtained results. Hyperparameters for all models were optimized using Bayesian optimization over 30 iterations, as shown in Table 1. This optimization significantly improved the accuracy in most models. The Bayesian optimization algorithm aims to minimize a scalar objective function f(x) within a bounded domain, whether deterministic or stochastic. It utilizes a Gaussian process model of the objective function f(x) and a Bayesian update procedure for modifying the model at each new evaluation. The acquisition function a(x) is then maximized to determine the next evaluation point x. This process begins by evaluating several random points within the variable bounds, then iteratively updating the Gaussian process model, and selecting new points based on the acquisition function. The algorithm stops after a fixed number of iterations (30 by default) or upon meeting other stopping criteria. This method effectively balances exploration and exploitation, leading to robust and well-performing models, ultimately enhancing the predictive accuracy (Bull, 2011; Snoek, Larochelle, & Adams, 2012). Table 1 also describes the hyperparameters that should be optimized for each type of model and the search range of each hyperparameter.

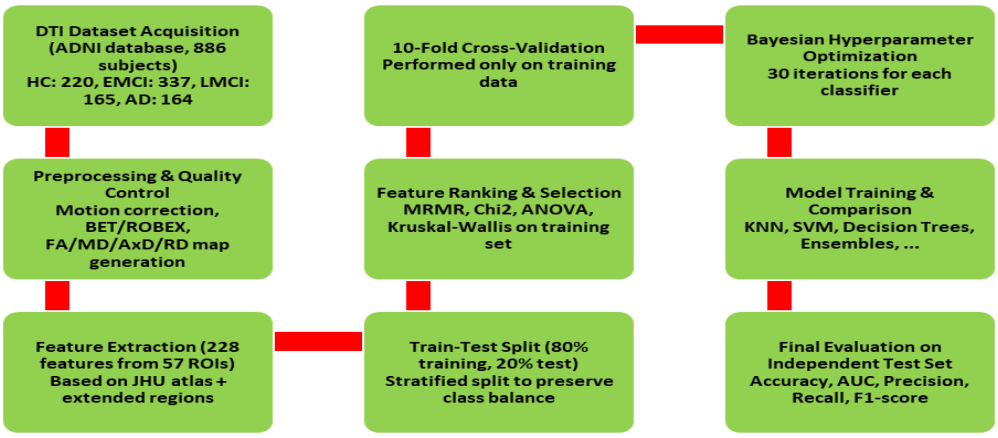

Figure 1. Overview of the proposed machine learning pipeline for Alzheimer's disease classification using DTI-derived features

Among the classification models in Table 1, the KNN achieved the highest overall accuracy in the four-class classification task, with validation and test accuracies of 92.5% and 90.4%, respectively. Figure 2 illustrates the Receiver Operating Characteristic (ROC) curve, Precision-Recall curve, and confusion matrix for the KNN on the test set.

Feature ranking methods—including MRMR, Chi-squared (Chi2), ANOVA, and Kruskal-Wallis—were utilized to evaluate and prioritize the importance of the input features. Each method applies a distinct statistical approach, enabling a thorough and complementary assessment of the feature relevance (Hogg & Ledolter, 1987; Ding & Peng, 2005). Each algorithm employs a distinct strategy for assessing the feature importance, collectively enabling a more comprehensive analysis. MRMR focuses on selecting features that are maximally relevant yet minimally redundant. Chi2 is a statistical test used to determine if there is a significant association between the categorical variables. ANOVA compares the means of different groups to ascertain if any of them differ significantly. The Kruskal-Wallis test, on the other hand, is a non-parametric method used for comparing more than two samples that are independent, or not related. The top-ranked features are presented in Table 2, revealing a consistent pattern of importance across all four algorithms. Notably, AxD_UNC_L emerged as the most significant feature, consistently receiving the highest rank.

Table 1. Bayesian optimization for finding optimum values of hyperparameters of different models for classification of HC, EMCI, LMCI, and AD groups

Model	Hyperparameters			Accuracy (Validation)	Accuracy (Test)	Prediction speed (obs/sec)	Training time (sec)	Model size (Compact) (kB)
	Name	Search range	Optimized value					
Optimizable Tree	Maximum number of splits	1 - 708	106	59.8	52.5	2100	131.6	66
	Split criterion	Gini's diversity index, Twoing rule, Maximum deviance reduction	Twoing rule					
Optimizable Discriminant	Discriminant type	Linear, Quadratic, Diagonal Linear, Diagonal Quadratic	Linear	62.1	64.4	1900	111.22	877
Optimizable Naïve Bayes	Distribution names	Gaussian, Kernel	Kernel	42.7	42.4	61	2323.4	7000
	Kernel type	Gaussian, Box, Epanechnikov, Triangle	Gaussian					
	Standardize data	true, false	No					
Optimizable SVM	Multiclass coding	One-vs-All, One-vs-One	One-vs-All	88.3	87	1600	2006.3	2000
	Box constraint level	0.001-1000	0.0010607					
	Kernel scale	0.001 – 1000	-					
	Kernel function	Gaussian, Linear, Quadratic, Cubic	Quadratic					
	Standardize data	true, false	Yes					
Optimizable Efficient Linear	Learner	SVM, Logistic regression	SVM	47	40.7	1900	414.42	216
	Regularization	Ridge, Lasso	Ridge					
	Regularization strength (Lambda)	1.4104e-08 – 141.0437	17.2405					
	Multiclass coding	One-vs-All, One-vs-One	One-vs-All					
Optimizable KNN	Number of neighbors	1 – 355	1	**92.5**	**90.4**	740	254.16	1000
	Distance metric	City block, Chebyshev, Correlation, Cosine, Euclidean, Hamming, Jaccard, Mahalanobis, Minkowski (cubic), Spearman	Cosine					

	Distance weight	Equal, Inverse, Squared inverse	Squared Inverse					
	Standardize data	true, false	Yes					
Optimizable Kernel	Learner	SVM, Logistic regression	SVM	85.3	83.1	800	2164.7	463
	Number of expansion dimensions	100 – 10000	231					
	Regularization strength (Lambda)	1.4104e-06 – 1.4104	1.2295					
	Kernel scale	0.001 – 1000	0.0010638					
	Multiclass coding	One-vs-All, One-vs-One	One-vs-All					
	Standardize data	true, false	Yes					
Optimizable Ensemble	Ensemble method	Bag, AdaBoost, RUSBoost	AdaBoost	86.5	81.9	120	4391.5	29000
	Number of learners	10 – 500	486					
	Learning rate	0.001 – 1	0.93892					
	Maximum number of splits	1 – 708	77					
	Number of predictors to sample	1 – 228	-					

4. Discussions

The results in Table 1 demonstrate the efficacy of using DTI metrics as features for classifying different stages of the AD. The Optimizable KNN model achieved the highest test accuracy (90.4%) among all models, highlighting its exceptional ability to classify the AD stages. This performance is attributed to the optimized hyperparameters, including the use of a Cosine distance metric, one neighbor, and squared inverse distance weighting, which likely enhanced the model's ability to discriminate between the subtle class differences. Similarly, the Optimizable SVM with a quadratic kernel function and One-vs-All multiclass coding achieved a high test accuracy of 87%. The kernel's non-linear decision boundaries effectively captured the complex relationships in the data, making it one of the top-performing models. In contrast, the Optimizable Naïve Bayes classifier, despite using a kernel distribution achieved a relatively low test accuracy (42.4%), indicating its limited suitability for this dataset. The use of the kernel-based probability estimation increased the computational complexity, as evidenced by the significant training time (2323.4 seconds) and the large model size (7,000 kB).

The prediction speed varied significantly across models, reflecting the differences in the computational demands. The Optimizable Discriminant model exhibited the highest prediction speed (1,900 obs/sec), making it ideal for the real-time or large-scale applications. This can be attributed to its linear discriminant type, which simplifies the decision boundaries. In contrast, the Optimizable Ensemble model demonstrated the slowest prediction speed (120 obs/sec), reflecting the computational cost of its AdaBoost method, high number of learners (486), and large model size (29,000 kB). The training time was shortest for the models with fewer parameters and simpler structures. For instance, the Optimizable KNN model trained in just 254.16 seconds, benefiting from its reliance on a single neighbor and correlation distance metric. On the other hand, the Optimizable Kernel model had one of the longest training times (2,164.7 seconds), primarily due to its high dimensionality (231 expansion dimensions) and the computational expense of the SVM kernel calculations. The Optimizable Efficient Linear model demonstrated one of the smallest

model sizes (216 kB), making it suitable for the lightweight applications. In contrast, the Optimizable Ensemble model had a significantly larger size (29,000 kB), reflecting its complexity and reliance on multiple base learners. Similarly, the Optimizable Naïve Bayes model (7,000 kB) was also large, limiting its practicality for the resource-constrained deployments.

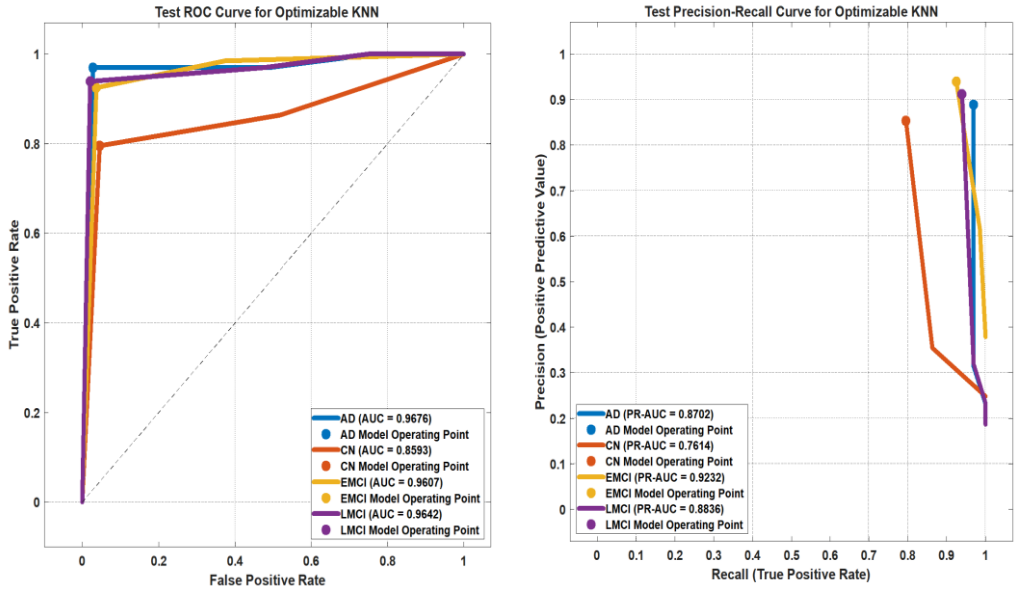

(a) (b)

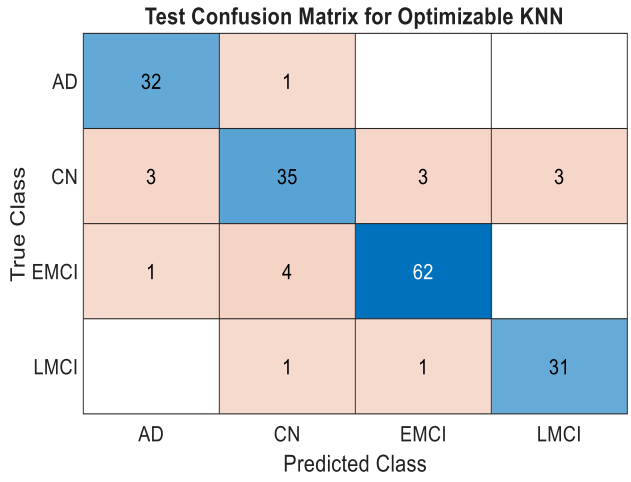

(c)

Figure 2. Different performance metrics of the KNN model in classification of HC, EMCI, LMCI, and AD groups: a) ROC curve, b) Precision-Recall curve, c) Confusion matrix

The results highlight the trade-offs between accuracy, computational efficiency, and resource requirements; the Optimizable KNN provides an unparalleled accuracy but requires moderate computational resources, making it suitable for the high-stakes diagnostic tasks. The Optimizable SVM offers a balance of high accuracy and moderate prediction speed, excelling in the scenarios where accuracy is paramount but resources are less constrained. The Optimizable Discriminant is ideal for the real-time applications due to its high prediction speed and compact model size, despite its slightly lower accuracy compared to KNN and SVM. The Optimizable Ensemble achieves high accuracy but at the expense of slow predictions, long training times, and large model sizes, limiting its use to offline analysis or research applications. The findings emphasize the importance of aligning model selection with application requirements, balancing accuracy with computational efficiency and scalability.

Table 2. Top ten features with higher importance values in each feature ranking method.

MRMR	Chi2	ANOVA	Kruskal Wallis
AxD_UNC_L	AxD_UNC_L	AxD_UNC_L	AxD_UNC_L
FA_PCR_L	AxD_UNC_R	RD_SS_L	MD_SS_L
FA_SCP_R	RD_SS_L	MD_SS_L	RD_SS_L
AxD_FX_L	MD_UNC_L	MD_UNC_L	AxD_UNC_R
FA_IFO_L	MD_UNC_R	AxD_SS_L	MD_UNC_L
AxD_SS_L	MD_SS_L	MD_CGH_L	MD_CGH_L
AxD_UNC_R	MD_CGH_L	RD_UNC_L	AxD_CGH_L
FA_ALIC_R	AxD_SS_L	AxD_CGH_L	AxD_SS_L
AxD_CGH_L	RD_UNC_L	RD_CGH_L	RD_CGH_L
FA_FX_L	RD_CGH_L	AxD_UNC_R	MD_UNC_R

AxD_UNC_L: AxD Uncinate fasciculus left, FA_PCR_L: FA Posterior corona radiata left, FA_SCP_R: FA Superior cerebellar peduncle right, AxD_FX_L: AxD Fornix left, FA_IFO_L: FA Inferior fronto-occipital fasciculus left, AxD_SS_L: AxD Sagittal stratum left, AxD_UNC_R: AxD Uncinate fasciculus right, FA_ALIC_R: FA Anterior limb of internal capsule right, AxD_CGH_L: AxD Cingulum (hippocampus) left, FA_FX_L: FA Fornix left, RD_SS_L: RD Sagittal stratum left, MD_UNC_L: MD Uncinate fasciculus left, MD_UNC_R: MD Uncinate fasciculus right, MD_SS_L: MD Sagittal stratum left, MD_CGH_L: MD Cingulum (hippocampus) left, RD_UNC_L: RD Uncinate fasciculus left, RD_CGH_L: RD Cingulum (hippocampus) left

The ROC curves presented in Figure 2a demonstrate the KNN model's capacity for distinguishing between the diagnostic groups. Notably, the model achieved high AUC values for AD, EMCI, and LMCI, with AUCs of 0.9676, 0.9607, and 0.9642, respectively, indicating excellent discriminatory power for these classifications. In contrast, the classification of HC showed a slightly lower AUC of 0.8593, suggesting a relatively reduced capacity to differentiate this group from others. The operating points on the ROC curves further specify the sensitivity and specificity trade-off achieved by the model for each group. Overall, while the model exhibits strong performance across all groups, the nuanced differences in the AUC values suggest potential variations in the model's ability to precisely classify individuals within the spectrum of the cognitive decline. Similarly, the Precision-Recall curves (Figure 2b) illustrate a favorable balance between the model's ability to correctly identify the positive cases and avoid the false positives. The confusion matrix (Figure 2c) provides a detailed breakdown of the classification outcomes, highlighting the number of true positives, true negatives, false positives, and false negatives for each group. This allows for a granular understanding of the model's strengths and weaknesses in correctly assigning individuals to their respective diagnostic categories.

A striking observation from Table 2 is the consistent prominence of the Axial Diffusivity (AxD) of the left Uncinate fasciculus (AxD_UNC_L), which appears as the top-ranked feature in all four methods. This high degree of consensus across diverse statistical approaches underscores its critical role. The uncinate fasciculus (UNC) is a major white matter tract connecting the anterior temporal lobe and the orbitofrontal cortex, playing a crucial role in various cognitive functions, including memory, emotion regulation, and language processing. The abnormalities in the UNC, as reflected by the changes in DTI metrics like AxD, have been implicated in several neurological and psychiatric conditions. The axial diffusivity (AxD) generally reflects the axonal integrity, and a decrease in the AxD can suggest the axonal damage or demyelination, while an increase might indicate an axonal swelling or early Wallerian degeneration (Acosta-Cabronero et al., 2012;

Salvadores, Gerónimo-Olvera, & Court, 2020).

Beyond AxD_UNC_L, several other features demonstrate their high importance across multiple methods, suggesting their robust association with the underlying phenomenon being investigated. Both Radial Diffusivity (RD_SS_L) and Mean Diffusivity (MD_SS_L) of the left sagittal stratum are frequently identified. The sagittal stratum is a broad white matter sheet containing several major association and projection fibers, including the inferior fronto-occipital fasciculus and the inferior longitudinal fasciculus, which are vital for the visual processing, language, and executive functions. RD is often considered sensitive to demyelination, while MD is a general measure of water diffusion, reflecting the overall tissue integrity (Nir et al., 2013; Zhang et al., 2014). In addition to AxD_UNC_L, the right uncinate fasciculus (AxD_UNC_R, MD_UNC_R) and the left uncinate fasciculus (MD_UNC_L, RD_UNC_L) also appear, further emphasizing the bilateral importance of this tract. The left cingulum (hippocampus) (AxD_CGH_L, MD_CGH_L, RD_CGH_L) is another recurrent feature. The cingulum bundle, particularly its hippocampal portion, is integral to the limbic system, involved in memory, emotion, and executive control (Song et al., 2002; Dou et al., 2020). The left fornix (AxD_FX_L, FA_FX_L) is also present in some rankings. The fornix is a C-shaped bundle of nerve fibers in the brain that acts as the primary efferent pathway from the hippocampus, playing a critical role in memory formation and recall (Zhang et al., 2014). FA_ALIC_R and FA_PCR_L appear in some rankings. These structures contain projection fibers connecting the cerebral cortex to the subcortical structures and the brainstem, involved in the motor and sensory pathways.

Recent research has increasingly applied DTI and machine learning for Alzheimer's disease classification, though most studies focus on a binary classification or require multimodal imaging. For example, Ren et al. combined the DTI features with clinical scores such as MMSE and ADAS, achieving 97.8% accuracy in AD vs. HC classification (Ren et al., 2023). Similarly, Song et al. employed graph-based white matter networks from DTI to predict MCI-to-AD conversion with an AUC of 0.92 (Song et al., 2024). Pan et al. used a cross-modal transformer GAN to fuse DTI with the resting-state fMRI for their multiclass classification, yielding strong results but depending on complex multimodal data (Pan et al., 2024). Yang et al. adopted the white matter connectivity networks derived from DTI and used SVM-RBF to classify AD, MCI, and HC, achieving high accuracy but limited in handling class imbalance (Yang et al., 2023). Hechkel & Helati (2025) developed a deep learning model using fused DTI and T1-weighted MRI data, obtaining a robust binary classification performance, but without exploring the intermediate disease stages (Hechkel & Helali, 2025). In contrast, the present work addresses the more challenging four-class classification task (HC, EMCI, LMCI, AD) using only DTI-derived features across 57 ROIs. Additionally, a misclassification cost matrix was incorporated to mitigate the effects of class imbalance, particularly for the AD and LMCI classes. These results are comparable to or exceed the recent multimodal or binary studies, demonstrating that the carefully optimized DTI-based pipelines, paired with the cost-sensitive learning, can deliver an accurate and clinically relevant multi-stage AD classification.

5. Conclusion

This study successfully demonstrated the utility of the Diffusion Tensor Imaging (DTI) metrics, particularly the Axial Diffusivity (AxD) in the left uncinate fasciculus, as robust biomarkers for classifying various stages of Alzheimer's disease (AD), including the Early and Late Mild Cognitive Impairment (EMCI, LMCI), and differentiating them from the healthy controls. Through the application of the optimized machine learning techniques, notably the K-Nearest Neighbors (KNN) model which achieved a 90.4% accuracy, these findings underscore the significant potential of the DTI-derived features for enhancing the multi-stage AD diagnosis. This work contributes to a deeper understanding of the neuropathological mechanisms underlying the AD progression and offers a promising non-invasive approach for earlier and more precise clinical assessment.

Acknowledgments

This research was supported by the Iran National Science Foundation (INSF), grant number 96000741.

REFERENCES

Acosta-Cabronero, J., Alley, S., Williams, G.B., Pengas, G. & Nestor, P.J. (2012) Diffusion Tensor Metrics as Biomarkers in Alzheimer's Disease. *PLoS One.* 7(11), e49072. doi:10.1371/journal.pone.0049072.

Albert, M.S., DeKosky, S.T., Dickson, D., Dubois, B., Feldman, H.H., Fox, N.C., Gamst, A., Holtzman, D.M., Jagust, W.J., Petersen, R.C., Snyder, P.J., Carrillo, M.C., Thies, B. & Phelps, C.H. (2011) The diagnosis of mild cognitive impairment due to Alzheimer's disease: recommendations from the National Institute on Aging-Alzheimer's Association workgroups on diagnostic guidelines for Alzheimer's disease. *Alzheimers Demen.* 7(3), 270-279. doi: 10.1016/j.jalz.2011.03.008.

Basser, P.J., Mattiello, J. & LeBihan, D. (1994) MR diffusion tensor spectroscopy and imaging. *Biophysical Journal.* 66(1), 259-267. doi: 10.1016/s0006-3495(94)80775-1.

Bull, A.D. (2011) Convergence Rates of Efficient Global Optimization Algorithms. *Journal of Machine Learning Research.* 12(88), 2879-2904.

Chandra, A., Dervenoulas, G. & Politis, M. (2019) Magnetic resonance imaging in Alzheimer's disease and mild cognitive impairment. *Journal of Neurology.* 266(6), 1293-1302. doi:10.1007/s00415-018-9016-3.

Ding, C. & Peng, H. (2005) Minimum redundancy feature selection from microarray gene expression data. *Journal of Bioinformatics and Computational Biology*. 3(2), 185-205. doi:10.1142/s0219720005001004.

Dou, X., Yao, H., Feng, F., Wang, P., Zhou, B., Jin, D., Yang, Z., Li, J., Zhao, C., Wang, L., An, N., Liu, B., Xi, Z. & Liu, Y. (2020) Characterizing white matter connectivity in Alzheimer's disease and mild cognitive impairment: An automated fiber quantification analysis with two independent datasets. *Cortex.* 129, 390-405. doi: 10.1016/j.cortex.2020.03.032.

Hechkel, W. & Helali, A. (2025) Early detection and classification of Alzheimer's disease through data fusion of MRI and DTI images using the YOLOv11 neural network. *Frontiers in Neuroscience.* 19. 1-12. doi: 10.3389/fnins.2025.1554015.

Hogg, R. V. & Ledolter, J. (1987) *Engineering statistics.* New York: Macmillan, London: Collier Macmillan. Pages 420.

Hojjati, S.H., Ebrahimzadeh, A., Khazaee, A. & Babajani-Feremi, A. (2018) Predicting conversion from MCI to AD by integrating rs-fMRI and structural MRI. *Computers in Biology and Medicine.* 102, 30-39. doi:10.1016/j.compbiomed.2018.09.004.

Holmes, C.J., Hoge, R., Collins, L., Woods, R., Toga, A.W. & Evans, A. C. (1998) Enhancement of MR images using registration for signal averaging. *Journal of Computer Assisted Tomography.* 22(2), 324-333. doi:10.1097/00004728-199803000-00032.

Hosmer Jr., D.W., Lemeshow, S. & Sturdivant, R.X. (2013) *Applied logistic regression*. Haboken, New Jersey, SUA: John Wiley & Sons, Inc.

Iglesias, J.E., Liu, C.-Y., Thompson, P.M. & Tu, Z. (2011) Robust brain extraction across datasets and comparison with publicly available methods. *IEEE Transactions on Medical Imaging.* 30(9), 1617-1634. doi:10.1109/TMI.2011.2138152.

Jack, C.R. Jr, Bernstein, M.A., Fox, N.C., Thompson, P., Alexander, G., Harvey, D., Borowski, B., Britson, P.J., Whitwell, J.L., Ward, C., Dale, A.M., Felmlee, J.P., Gunter, J.L., Hill, D.L., Killiany, R., Schuff, N., Fox-Bosetti, S., Lin, C., Studholme, C., DeCarli, C.S., Krueger, G., Ward, H.A., Metzger, G.J., Scott, K.T., Mallozzi, R., Blezek, D., Levy, J., Debbins, J.P., Fleisher, A.S., Albert, M., Green, R., Bartzokis, G., Glover, G., Mugler, J . & Weiner, M.W. (2008) The Alzheimer's Disease Neuroimaging Initiative (ADNI): MRI methods. *Journal of Magnetic Resonance Imaging.* 27(4), 685-691. doi:10.1002/jmri.21049.

Jack, C.R., Jr., Knopman, D.S., Jagust, W.J., Shaw, L.M., Aisen, P.S., Weiner, M.W., Petersen, R.C. & Trojanowski, JQ. (2010) Hypothetical model of dynamic biomarkers of the Alzheimer's pathological cascade. *Lancet. Neurol.* 9(1), 119-128. doi:10.1016/s1474-4422(09)70299-6.

Jenkinson, M., Bannister, P., Brady, M. & Smith, S. (2002) Improved Optimization for the Robust and Accurate Linear Registration and Motion Correction of Brain Images. *Neuroimage.* 17(2), 825-841. doi:10.1006/nimg.2002.1132.

Khazaee, A., Ebrahimzadeh, A. & Babajani-Feremi, A. (2015) Identifying patients with Alzheimer's disease using resting-state fMRI and graph theory. *Clinical Neurophysiology.* 126(11), 2132-2141. doi:10.1016/j.clinph.2015.02.060.

Khazaee, A., Ebrahimzadeh, A. & Babajani-Feremi, A. (2017) Classification of patients with MCI and AD from healthy controls using directed graph measures of resting-state fMRI. *Behavioul Brain Research.* 322(Pt B), 339-350. doi:10.1016/j.bbr.2016.06.043.

Le Bihan, D., Mangin, J.F., Poupon, C., Clark, C.A., Pappata, S., Molko, N. & Chabriat, H. (2001) Diffusion tensor imaging: Concepts and applications. *Journal of Magnetic Resonance Imaging.* 13(4), 534-546. doi:10.1002/jmri.1076.

Leow, A.D., Yanovsky, I., Chiang, M.-C., Lee, A.D., Klunder, A.D., Lu, A., Becker, T.J., Davis, S.W., Toga, A.W. & Thompson, P.M. (2007) Statistical Properties of Jacobian Maps and the Realization of Unbiased Large-Deformation Nonlinear Image Registration. *IEEE Transactions on Medical Imaging.* 26(6), 822-832. doi:10.1109/tmi.2007.892646.

Mori, S., Oishi, K., Jiang, H., Jiang, L., Li, X., Akhter, K., Hua, K., Faria, A.V., Mahmood, A., Woods, R., Toga, A.W., Pike, G.B., Neto, P.R., Evans, A., Zhang, J., Huang, H., Miller, M.I., van Zijl, P., & Mazziotta, J. (2008) Stereotaxic white matter atlas based on diffusion tensor imaging in an ICBM template. *NeuroImage.* 40(2), 570-582. doi:10.1016/j.neuroimage.2007.12.035.

Mori, S. & Zhang, J. (2006) Principles of Diffusion Tensor Imaging and Its Applications to Basic Neuroscience Research. *Neuron.* 51(5), 527-539. doi:10.1016/j.neuron.2006.08.012.

Nir, T.M., Jahanshad, N., Villalon-Reina, J.E., Toga, A.W., Jack, C.R., Weiner, M.W. & Thompson, P.M. (2013) Effectiveness of regional DTI measures in distinguishing Alzheimer's disease, MCI, and normal aging. *NeuroImage Clinical.* 3, 180-195. doi:10.1016/j.nicl.2013.07.006.

Pan, J., Jing, C., Zuo, Q., Nieuwoudt, M. & Wang, S. (2024) Cross-Modal Transformer GAN: A Brain Structure-Function Deep Fusing Framework for Alzheimer's Disease. In *Lecture Notes in Computer Science Advances in Brain Inspired Cognitive Systems*. pp. 82-92. Springer Nature, Singapore.

Petersen, R.C., Smith, G.E., Waring, S.C., Ivnik, R.J., Tangalos, E.G. & Kokmen, E. (1999) Mild cognitive impairment: clinical characterization and outcome. *Archives of Neurology.* 56(3), 303-308. doi:10.1001/archneur.56.3.303.

Rahimi, A. & Recht, B. (2007) Random features for large-scale kernel machines. In: Platt, J., Koller, D., Singer, Y. & Roweis, S. (eds.) *Advances in neural information processing systems (NIPD 2007)*, Volume 20. Curran Associates, Inc.

Ren, Z., Yao, X., Yuan, Z. & Zhou, L. (2023) Machine Learning Classification of Alzheimer's Disease Using Joint Features of Diffusion Tensor Imaging and Clinical Scales. In *Proceedings of International Conference on Image, Vision and Intelligent Systems 2022 (ICIVIS 2022)*, Series Lecture Notes in Electrical Engineering, Singapore. pp. 320-327.

Rish, I., Hellerstein, J. & Thathachar, J. (2001) An analysis of data characteristics that affect naive Bayes performance. *IBM TJ Watson Research Center.* 30, 1-8.

Salvadores, N., Gerónimo-Olvera, C. & Court, F.A. (2020) Axonal Degeneration in AD: The Contribution of Aβ and Tau. *Frontiers in Aging Neuroscience.* 12(581767), 1-16. doi:10.3389/fnagi.2020.581767.

Seiffert, C., Khoshgoftaar, T. M., Van Hulse, J. & Napolitano, A. (2010) RUSBoost: A Hybrid Approach to Alleviating Class Imbalance. *IEEE Transactions on Systems, Man, and Cybernetics-Part A: Systems and Humans.* 40(1), 185-197. doi:10.1109/TSMCA.2009.2029559.

Smith, S.M. (2002) Fast robust automated brain extraction. *Human Brain Mapping.* 17(3), 143-155. doi:10.1002/hbm.10062.

Snoek, J., Larochelle, H. & Adams, R.P. (2012) Practical bayesian optimization of machine learning algorithms. In: Pereira, F., Burges, C.J., Bottou, L. & Weinberger, K.Q. (eds.) *Advances in neural information processing system (NIPS 2012)*. 25, 1-9. Curran Associates, Inc.

Song, Q., Peng, J., Shu, Z., Xu, Y., Shao, Y., Yu, W. & Yu, L. (2024) Predicting Alzheimer's progression in MCI: a DTI-based white matter network model. *BMC Medical Imaging.* 24(103), 1-9. doi:10.1186/s12880-024-01284-7.

Song, S. K., Sun, S. W., Ramsbottom, M. J., Chang, C., Russell, J. & Cross, A. H. (2002) Dysmyelination revealed through MRI as increased radial (but unchanged axial) diffusion of water. *NeuroImage.* 17(3), 1429-1436. doi:10.1006/nimg.2002.1267.

Sperling, R.A., Aisen, P.S., Beckett, L.A., Bennett, D. A., Craft, S., Fagan, A.M., Iwatsubo, T., Jack, C.R. Jr., Kaye, J., Montine, T.J., Park, D.C., Reiman, E.M., Rowe, C.C., Siemers, E., Stern, Y., Yaffe, K., Carrillo, M.C., Thies, B., Morrison-Bogorad, M., Wagster, M.V. & Phelps, C.H. (2011) Toward defining the preclinical stages of Alzheimer's disease: recommendations from the National Institute on Aging-Alzheimer's Association workgroups on diagnostic guidelines for Alzheimer's disease. *Alzheimers Dement.* 7(3), 280-292. doi:10.1016/j.jalz.2011.03.003.

Stebbins, G.T. & Murphy, C.M. (2009) Diffusion tensor imaging in Alzheimer's disease and mild cognitive impairment. *Behavioural Neurology.* 21(1), 39-49. doi:10.3233/ben-2009-0234.

Sun, S.W., Liang, H.F., Le, T.Q., Armstrong, R.C., Cross, A.H. & Song, S.-K. (2006) Differential sensitivity of in vivo and ex vivo diffusion tensor imaging to evolving optic nerve injury in mice with retinal ischemia. *NeuroImage*. 32(3), 1195-1204. doi:10.1016/j.neuroimage.2006.04.212.

Yang, X., Xia, Y., Li, Z., Liu, L., Fan, Z. & Zhou, J. (2023) Classification of Alzheimer's Disease Based on White Matter Connectivity Network. *Applied Sciences*. 13(21), 12030. doi:10.3390/app132112030.

Zhang, B., Xu, Y., Zhu, B. & Kantarci, K. (2014) The role of diffusion tensor imaging in detecting microstructural changes in prodromal Alzheimer's disease. *CNS Neuroscience & Therapeutics*. 20(1), 3-9. doi:10.1111/cns.12166.

Ali KHAZAEE is an Assistant Professor at the University of Bojnord, Iran. He holds a Ph.D. in Electrical and Communication Engineering, with a research focus on advancing brain disease diagnostics and treatments. His areas of expertise include biomedical signal processing, neuroimaging, and artificial intelligence. Dr. Khazaee has published over 28 journal and conference papers, accumulating 1,824 citations and achieving an h-index of 15. He has supervised numerous graduate and undergraduate theses and serves as a reviewer for prestigious journals in neuroscience and medical imaging.

Abdolreza MOHAMMADI received the Ph.D. degree in communication systems engineering from Yazd University, Yazd, Iran. He is currently an Assistant Professor of electrical engineering at the University of Bojnord, Bojnord, Iran. His research interests include fuzzy probability, statistical signal processing, information fusion, and wireless sensor networks.